

***In vivo* measurements of the wavelength dependence of tissue-scattering coefficients between 760 and 900 nm measured with time-resolved spectroscopy**

S. J. Matcher, M. Cope, and D. T. Delpy

We present *in vivo* values for the optical transport coefficients (μ_a , μ_s') of the adult human forearm, calf, and head from 760 to 900 nm measured with time-resolved spectroscopy. The accuracy of the method is tested with tissue-simulating phantoms. We obtain $\mu_s'(\lambda) \approx 1.1 - (5.1 \times 10^{-4} \lambda) \text{ mm}^{-1}$ (forearm), $1.6 - (8.9 \times 10^{-4} \lambda) \text{ mm}^{-1}$ (calf), and $1.45 - (6.5 \times 10^{-4} \lambda) \text{ mm}^{-1}$ (head), where λ is measured in nanometers. At 800 nm we obtain $\mu_a = 0.023 \pm 0.004 \text{ mm}^{-1}$ (forearm), $0.017 \pm 0.005 \text{ mm}^{-1}$ (calf), and $0.016 \pm 0.001 \text{ mm}^{-1}$ (head). Our values differ substantially from published *in vitro* data. In particular, our transport coefficients for the adult head are substantially lower than previously reported values for adult human cerebral matter and pig skull cortical bone measured *in vitro*. © 1997 Optical Society of America

Key words: Tissue optical properties, time-resolved spectroscopy.

1. Introduction

Considerable interest in the optics community is focused currently on the propagation of optical and near-infrared radiation through living tissue because of the great promise of optical techniques for the non-invasive monitoring of tissue oxygenation with near-infrared spectroscopy, the noninvasive treatment of tumors with photodynamic therapy, and the optical imaging of tissue oxygenation.¹⁻⁶ Light propagation through body tissues is complicated by the fact that most tissues scatter optical and infrared radiation multiply because, in general, the transport scattering coefficient μ_s' is much larger than the absorption coefficient μ_a . Various mathematical models of tissue light propagation have been proposed,⁷ of which the diffusion approximation to the Boltzmann transport equation is currently the most popular. Regardless

of the particular light transport model employed, however, the accurate prediction of light flux distributions within body tissues depends crucially on the availability of accurate, preferably *in vivo*, estimates of the radiation transport coefficients μ_s' and μ_a . Recently, interest in the wavelength dependence of μ_s' has arisen through the possibility of the measurement of absolute hemoglobin saturation in the head when spatially resolved diffuse back reflectance is used to measure the tissue effective attenuation coefficient μ_{eff} .⁸⁻¹⁰ Knowledge of the wavelength dependence of the scattering coefficient $\mu_s'(\lambda)$ then allows the determination of the wavelength dependence of $\mu_a(\lambda)$, given $\mu_{\text{eff}}(\lambda)$, and hence estimation of the absolute mean hemoglobin saturation $S_m \text{O}_2$ [= $\text{HbO}_2 / (\text{Hb} + \text{HbO}_2)$].

A considerable literature exists on *in vitro* estimates of these parameters (e.g., a review by Cheong *et al.*¹¹), and many techniques have been proposed to determine the optical properties of postmortem tissue samples. These techniques include the modeling of diffuse reflectance and transmittance,¹² measurement of the optical attenuation coefficient of thin tissue samples,¹³ measurement of the spatial variation of tissue diffuse reflectance,¹⁴ and, more recently, measurements of tissue coherent backscatter^{15,16} and of the backscattered power in low-coherence reflectometry.¹⁷ Time-resolved spectroscopy,¹⁸ in which the

When this research was undertaken, all the authors were with the Department of Medical Physics and Bioengineering, University College, London, 1st Floor Shropshire House, 11-20 Copper Street, London WC1E 6JA UK. S. J. Matcher is currently with the Department of Physics, University of Exeter, Stocker Road, Exeter EX4 4QL UK.

Received 29 August 1995; revised manuscript received 15 May 1996.

0003-6935/97/010386-11\$10.00/0

© 1997 Optical Society of America

temporal broadening of an ultrashort light pulse is measured and modeled, has attracted interest as a rapid, noninvasive way of determining tissue optical properties *in vivo*.

Time-resolved spectroscopy involves the measurement of the effective tissue impulse response (the temporal point-spread function or TPSF) and the fit of this measured function with that predicted by a suitable model of light propagation in the tissue. Iterative improvement of the fit between the data and the model as μ_a and μ_s' are varied allows these parameters to be estimated. The technique offers several advantages over other methods for the determination of tissue optical properties:

(1) The technique can be applied readily to intact tissue, allowing *in vivo* measurements.

(2) The method determines directly the reduced scattering coefficient μ_s' unlike techniques involving the measurement of μ_s and the scattering anisotropy factor g in separate experiments. Biological scatterers generally have g values close to unity (i.e., they predominantly scatter light in the forward direction) so that extremely high precision becomes necessary in the estimation of g so as to obtain a reasonable precision in the estimate of μ_s' [$\mu_s' = \mu_s(1 - g)$].

(3) The method can be applied across significant thicknesses of tissue (several centimeters) and should thus provide an estimate of the bulk optical properties of the tissue. In contrast, coherent backscatter techniques are sensitive only to the optical properties of the surface layer of the medium that is several scattering mean-free-paths thick.

Barilli *et al.* used this method to determine the *in vivo* scattering coefficient of adult human forearm tissue at a single wavelength (800 nm), employing a Monte-Carlo model of light propagation in tissue.¹⁹ Mitic *et al.* and Suzuki *et al.* employed a solution to the time-dependent diffusion equation derived by Patterson *et al.*¹⁸ to obtain *in vivo* estimates of μ_a and μ_s' at 800 nm for human breast tissue with a Ti:sapphire-streak camera system and a picosecond laser diode-time-to-amplitude converter detector system, respectively.^{20,21} Zaccanti *et al.* also used the Patterson equation to derive *in vivo* estimates for μ_a and μ_s' at 825 nm on the adult human head, calf, forearm, and bicep.²²

In this paper we also employ the diffusion theory relation derived by Patterson to obtain tissue optical properties for the human forearm, calf, and head at 10-nm intervals from 760 to 900 nm and report on the wavelength dependence and mean value of the scattering coefficient in this range.

2. Experimental Measurements

Measurements were made on healthy adult volunteers (age range 18–55); forearm data were obtained on five subjects over the full wavelength range, calf data on 11 subjects, and head data on seven subjects. Because of limitations in the wavelength tuning range of the Tsunami laser, the full wavelength range

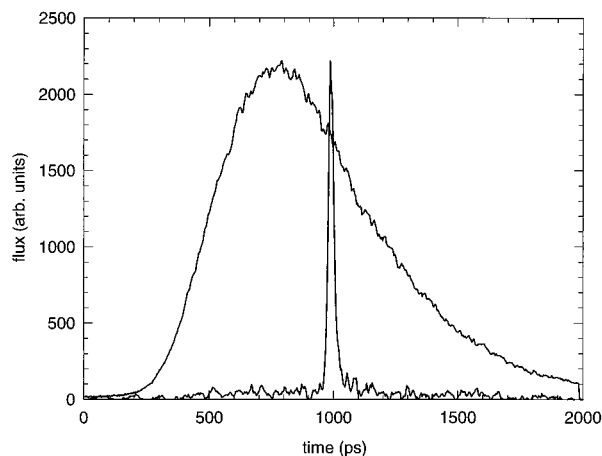


Fig. 1. Illustrative tissue TPSF and corresponding reference pulse profile as measured with a Hamamatsu C1385 streak camera and Spectra-Physics Tsunami Ti:Sapphire pulsed laser source.

actually had to be covered in two separate runs made several months apart. The first run covered the range of 760–840 nm. Then, following the acquisition of new laser optics, measurements covering the wavelength range of 800–900 nm were completed on the original volunteers.

The experimental setup used to acquire the data is described by Essenpreis *et al.*²³ Briefly, a pulsed mode-locked Ar⁺ pumped Ti:sapphire laser (Spectra-Physics, Ltd., Tsunami) was used to generate wavelength tunable pulses of duration <2 ps with a repetition rate of 82 MHz. These pulses were applied to the skin of the subjects' forearm, leg, and head with a low temporal dispersion graded-index optical fiber and the transmitted light collected by a bundle made from similar fiber placed approximately 4 cm away on the skin surface. The transmitted, temporally broadened laser pulse was imaged onto the photocathode of a synchroscan streak camera (Hamamatsu Photonics Ltd., C1385) and the resulting streak image was read out by an integral-cooled CCD camera. In addition to the transmitted pulse through the tissue, an optical reference pulse was also imaged onto the streak camera. Because this pulse propagates a known distance through air and glass, it provides a time reference and allows the absolute transit time of the transmitted pulse through the tissue to be determined. Because the reference pulse measures effectively the temporal impulse response of the laser-streak camera system, it can also be used in principle to deconvolve the measured tissue TPSF and thus improve the accuracy of the derived optical properties. In practice, the reference pulse is sufficiently narrow (<20 ps) with respect to the TPSF (>1 ns) that this step generally is judged superfluous. Figure 1 illustrates a typical measured TPSF and corresponding reference pulse. The reference pulse is generally arranged to arrive at the streak camera approximately 1 ns after the direct transmitted pulse arrives in the case that the delivery fiber is held directly in contact with the streak

camera detect fiber (with a piece of highly absorbing black card in between). Hence time zero is defined on the abscissa of the tissue TPSF as the time at which light enters the tissue.

3. Data Analysis

The format of the raw data from the streak camera CCD in the case of the wavelength-dependent measurements is two binary files, representing the intensity of light in the transmitted and reference pulses as a function of horizontal CCD pixel number (horizontal corresponding to the direction of sweep of the streak camera, i.e., the time axis). The sweep signal of the streak camera is derived from a 82-MHz sine-wave generator and so the rate of sweep (i.e., the time-base calibration measured in picoseconds per CCD pixel) varies noticeably during the sweep. The first step of data processing is thus to apply a previously determined nonlinear calibration to convert the abscissas from CCD pixels to picoseconds. This calibration also involves the rescaling of the detected intensities in each pixel to account for this variation in the rate of sweep. We accomplished the conversion of the abscissa of the tissue TPSF to absolute time by locating the peak signal in the reference pulse TPSF; the apparent time of occurrence of this peak minus the known offset of the reference pulse then defines time zero.

To obtain a simple, closed-form equation describing a tissue TPSF given the tissue μ_a and μ_s' and the source-detector spacing, we use the formula of Patterson *et al.*¹⁸:

$$R(t) = \frac{z_0}{(4\pi Dc)^{3/2}} t^{-5/2} \exp - \left(\frac{\rho^2 + z_0^2}{4Dct} \right) \exp(-\mu_a ct), \quad (1)$$

where R is the tissue reflectivity (ratio of reflected-to-input light intensity) as a function of time t , ρ is the source-detector spacing, z_0 is the effective isotropic source depth (approximately the reciprocal of μ_s'), D is the tissue diffusion coefficient $\{D = 1/[3(\mu_a + \mu_s')]\}$, and c is the velocity of light in the tissue.

This formula is derived with diffusion theory to calculate time-resolved diffuse reflectance from a semi-infinite half-space. The application of this formula to tissue structures such as the forearm, calf, and head thus requires the following simplifying assumptions:

- (1) The effects of curved boundaries affects the form of the TPSF negligibly.
- (2) The refractive index mismatch between tissue ($n_{\text{rel}} = 1.4$) and air ($n_{\text{rel}} = 1.0$) also has a negligible effect.
- (3) The tissue probed effectively can be considered homogeneous, i.e., possessing identical optical properties throughout its volume.

Because the source-detector spacing of 4 cm is comparable to the radius of curvature of the structures studied, assumption (1) may be a poor one and may lead to systematic errors in the derived μ_a and

μ_s' values. In phantom studies, Madsen *et al.* reported errors to 10% in the derivation of transport coefficients by the fitting of time-domain reflectance TPSF's, which they consider ascribable to such boundary geometry effects.²⁴ However, in this study we are interested mainly in the wavelength dependence of μ_s' , and the assumption that the systematic errors that are due to geometry are only weakly dependent on wavelength is likely to be a better assumption because, *a priori*, we anticipate μ_s' varying by 10% or less across the wavelength range.

Haskell *et al.* recently considered the effects of mismatched boundary conditions on the optical properties derived using the equivalent technique of phase-resolved spectroscopy.²⁵ They suggest that errors of around 10% may be induced if boundary reflections are neglected. Again, because tissue refractive index is only weakly dependent on wavelength, we anticipate little error in our derivation of the wavelength dependence of μ_s' . Our own results on tissues and tissuelike phantoms suggest that the relation derived by Haskell *et al.* will produce absolute μ_s' values less than 5% lower than by the use of the Patterson relation ($n_{\text{rel}} \approx 1.5$).

The problem of heterogeneity—specifically what interpretation to place on optical properties derived on the assumption that the tissue is homogeneous when, in the case of the head especially, it is not—is harder to address. However, we have reason to believe²⁶ that at 4-cm separation, near-infrared light mainly probes surface tissues (skin and skull) and the gray matter comprising the surface cerebral cortex of the brain. The derived parameters thus should be a function mainly of the optical properties of cortical bone and gray matter. *In vitro* measurements of the absorption and scattering coefficients of (blood-free) samples of pig cortical bone²⁷ and adult gray matter¹² yield values of μ_a , μ_s' of approximately 0.025, 1.8 and 0.032, 2.4 mm^{-1} , respectively, at 800 nm. If we adopt estimates of the total hemoglobin volume of 80 μM for the adult human brain and 40 μM for the skull, this will increase these values to 0.032, 1.8 and 0.047, 2.4 mm^{-1} , respectively. The precise relation we might expect between our derived values and these estimates (especially whether our values should lie between the above values for skull and gray matter) are discussed in Section 6.

4. Phantom Measurements

To verify the accuracy of the method and our system, we performed measurements on two tissue-simulating phantoms with:

- (a) A liquid phantom consisting of water and Intralipid-10% (Kabi Pharmacia) together with a molecular dye (ICI S109564) mixed together in a tank 100 mm \times 100 mm \times 70 mm to give estimated optical properties of $\mu_a = 0.027 \text{ mm}^{-1}$, $\mu_s' = 1 \text{ mm}^{-1}$ at 800 nm,²⁸ based on these Intralipid and dye concentrations.

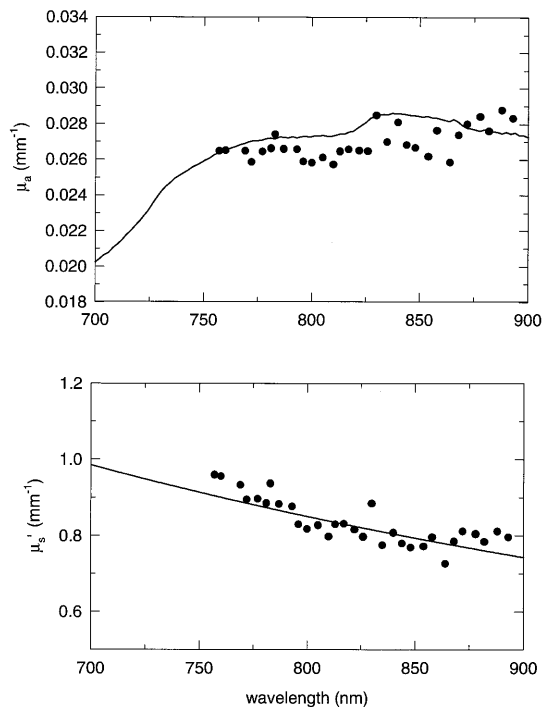


Fig. 2. $\mu_a(\lambda)$ and $\mu_s'(\lambda)$ measured on an Intralipid-10% and dye phantom. $\mu_a(\lambda)$ (solid circles) is compared with theory (solid curve) given the known absorption properties of water and the dye. $\mu_s'(\lambda)$ (scaled by a factor of 1.17) is compared with the data of van Stavaren *et al.* The wavelength dependence of μ_s' for Intralipid-10% measured in this study is in good agreement with van Stavaren *et al.*, but the absolute value is lower by approximately 20%.

(b) A solid phantom consisting of a polyester resin, dye, and titanium dioxide particles²⁹ with estimated optical properties of $\mu_a = 0.022 \text{ mm}^{-1}$, $\mu_s' = 0.91 \text{ mm}^{-1}$ at 800 nm, and of size $170 \text{ mm} \times 100 \text{ mm} \times 50 \text{ mm}$.

Time-resolved reflectance TPSF's were collected on the liquid and solid phantoms for source-detector spacings of 25 and 23.5 mm, respectively, in wavelength steps of 5 nm from approximately 750 to 890 nm. The small source-detector spacing made this feasible without the need for a mirror change, as the loss of laser efficiency at low wavelengths was not problematic. Identical data analysis steps were applied to these TPSF's as to the *in vivo* TPSF's. It was found necessary to include a correction for the wavelength dependence of the refractive index of the 3-m length of delivery fiber which introduced a significant change in the apparent time offset between object and reference laser pulses as the wavelength was varied.

Figure 2 shows the resulting $\mu_a(\lambda)$ and $\mu_s'(\lambda)$ for the Intralipid phantom. The derived μ_s' at 800 nm was found to underread the value quoted by van Stavaren *et al.*²⁸ (1 mm^{-1}) by approximately 20%. The solid curve thus represents the theoretical predictions of van Stavaren *et al.* scaled by a factor of 1.17, from which it can be seen that the wavelength

dependence of μ_s' is in good agreement with theory. In regard to the possible underread of the absolute value of μ_s' at 800 nm, unfortunately some doubt exists concerning whether Intralipid truly can be regarded as a gold standard scattering material for use in phantoms. Pan *et al.*, for example, while in agreement with van Stavaren *et al.* concerning the wavelength dependence of the unmodified scattering coefficient $\mu_s(\lambda)$, quote a value of μ_s' of approximately 0.52 mm^{-1} at 800 nm.³⁰ Allardice *et al.* also reported up to 10% variation in the μ_s of Intralipid—10% between different batches.³¹

Figure 3(a) shows similar results for the solid phantom. Here the estimate of μ_s' at 800 nm seems to be lower than the expected value for this phantom (based on Mie theory and given the particle-size distribution and refractive index of the titanium dioxide particles used as the scattering material) by approximately 5%. Again, however, the solid curves [representing the theoretical $\mu_a(\lambda)$ and $\mu_s'(\lambda)$ scaled to match the data] suggest that the wavelength dependence of the optical properties is measured accurately.

Unfortunately, the solid phantom suffers from a similar problem as the Intralipid phantom, namely, that there is some uncertainty in the absolute value of μ_s' , arising mainly from uncertainty in the value of g . We therefore need to know whether our technique systematically underreads μ_s' or whether the solid phantom actually has slightly different optical properties to its design specification. To answer this question we performed a further series of measurements of the spatial variation of diffuse back reflectance from a continuous light source. This technique was suggested by Patterson *et al.* as a means of estimating the effective attenuation coefficient $\mu_{\text{eff}}^* = [3\mu_a(\mu_a + \mu_s')]^{0.5}$ of a highly scattering medium.⁸ Figure 3(b) shows a comparison between μ_{eff} that we calculated from the μ_a , μ_s' values derived from the TPSF fitting with the value of μ_{eff} determined directly by scanning a fiber-optic bundle connected to a cooled CCD spectrometer³² across the surface of the solid phantom illuminated by a white-light source and a single fiber. One can see that the two measurements of μ_{eff} are in good agreement, which encourages us to believe that our measurement technique is accurate and that the previously described discrepancies with theory may result from inaccuracy of the prior knowledge of the optical properties of the phantoms.

5. Results

Figure 4 shows a representative fit between a tissue TPSF (measured across 4 cm of adult male forearm at 800 nm) and Eq. (1). The nonlinear least-squares fitting operation was performed with the Numerical Algorithms Group algorithm E04FDF.³³ We assumed that the errors on the data points were proportional to the square root of the signal intensity, an assumption that is valid when our streak camera is operating at its maximum gain and is then photon shot-noise limited. Note that because the precise

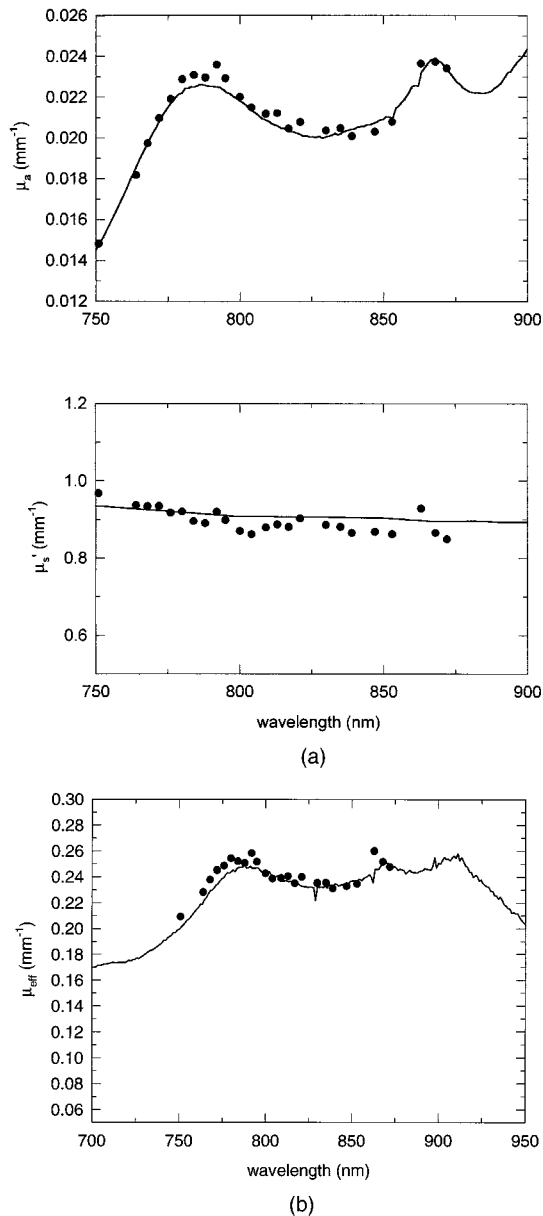


Fig. 3. (a) Same as for Fig. 2 but for measurements on a solid phantom consisting of titanium dioxide particles suspended in a polyester resin and dye mixture. The experimental μ_s' (solid circles) values have been scaled by a factor of 1.05 to compare their wavelength dependence with theoretical predictions (solid curve). (b) Comparison of the diffusion theory parameter $\mu_{\text{eff}} = [3\mu_a(\mu_a + \mu_s')]^{0.5}$ calculated from the μ_a , μ_s' values derived from TPSF fitting (solid circles) and measured directly by the measurement of the rate of change of light attenuation with respect to source-detector spacing (solid curve).

photoelectric gain of the streak camera-CCD system is generally unknown, one cannot estimate the absolute error on each data point by taking the square root of the signal intensity. This is not important for the weighted fitting procedure as the result is simply to scale χ^2 . Unfortunately it does preclude a direct estimation of the uncertainty of the derived μ_a and μ_s' values arising from measurement noise. Repeatability tests on stable phantoms, however, sug-

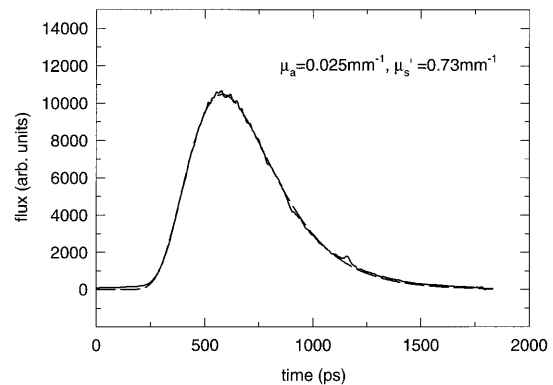


Fig. 4. Representative fit between a measured tissue TPSF (solid curve) and Eq. (1) (dashed curve) for the human forearm at 800 nm. The resulting fit parameters are $\mu_a = 0.025 \text{ mm}^{-1}$ and $\mu_s' = 0.73 \text{ mm}^{-1}$.

gest that this source of uncertainty is small compared with the observed intersubject variation, and so we quote the latter as the uncertainty of our values. The iterative minimization of χ^2 was begun from a starting point $\mu_a = 0.02 \text{ mm}^{-1}$, $\mu_s' = 0.5 \text{ mm}^{-1}$ in the case of the forearm data and 0.02 mm^{-1} and 1.0 mm^{-1} for the head and calf data. This procedure was repeated for all TPSF's measured on all subjects on the three tissue types (540 TPSF's in total), yielding estimates of μ_a and μ_s' as a function of wavelength for the adult head, forearm, and calf. The wavelength region 800–840 nm represents the overlap region between the data sets collected in the first run (760–840 nm) and those at the later date (800–900 nm). This break in the data sets unfortunately leads to a small discrepancy in the μ_a , μ_s' (and meantime) estimates obtained on identical subjects at the same wavelength between the two runs of approximately 10%. The cause of this is unknown, but is most likely due to small errors in the repositioning of the fibers (see below). Hence to estimate the wavelength dependence of μ_s' we introduced an *ad hoc* scaling factor to the 760–840-nm data set to make it match the 800–900-nm data set (derived by least-squares fitting the 760–840-nm data to the 800–900-nm data in the overlap region 800–840 nm). Figures 5(a)–5(c) show the results of this analysis. Visually the scattering coefficient spectra appear roughly linear, and so we have characterized the wavelength dependence of μ_s' by performing a linear regression on these spectra, i.e., representing the data by the relation $\mu_s'(\lambda) = a\lambda + b$. We then characterize the wavelength dependence by considering the slope-to-intercept ratio of this best-fit straight line (a/b). In Table 1 the results are tabulated for male and female forearm, male and female head, male and female calf, male calf, and female calf (the larger number of subjects in the leg study allows a meaningful segregation of the data). It is clear from the wavelength-dependence parameter $\langle a/b \rangle$ and its associated error that there is no statistically significant variation in the wavelength dependence of scattering coefficient between the three tissue types nor

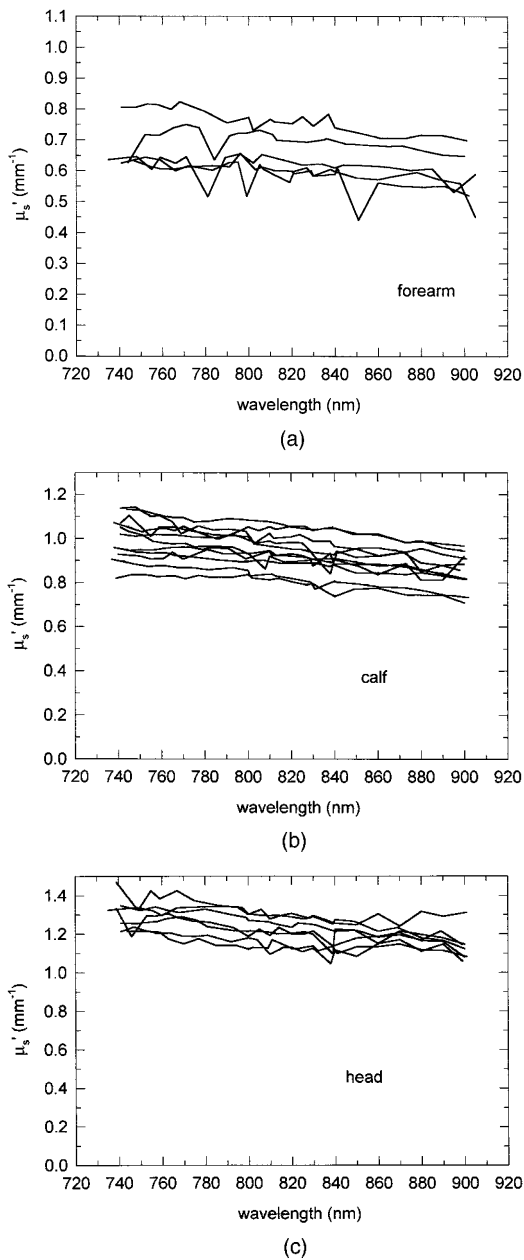


Fig. 5. Results of the μ_s' estimation procedure applied to tissue TPSF's collected on a number of adult volunteers across the wavelength range 760–900 nm. As described in the text, the 800–900-nm results were scaled to match the 760–840-nm data when we performed a linear least-squares fit of the former data set to the latter over the overlap region 800–840 nm. (a) $\mu_s'(\lambda)$ measured on the forearm of 5 volunteers, (b) $\mu_s'(\lambda)$ measured on the calf of 11 volunteers, (c) $\mu_s'(\lambda)$ measured on the head of 7 volunteers.

between male and female for the calf data. The head data appear to produce the lowest intersubject variability of both μ_s' and its wavelength dependence. The forearm data produce the highest variability of wavelength dependence, although the variability of absolute μ_s' at a single wavelength is somewhat lower than that of the calf data.

Because there was a small discrepancy between the estimates of absolute tissue μ_s' derived from the

Table 1. Intersubject Variability of the Wavelength Dependence of Scattering Coefficient^a

Tissue Type	<i>n</i>	$\langle a/b \rangle$	$\sigma(a/b)$	Variation (%)
Forearm, male and female	5	-4.7×10^{-4}	1.3×10^{-4}	28
Intact head, male and female	7	-4.6×10^{-4}	0.6×10^{-4}	13
Calf, male and female	11	-5.3×10^{-4}	1.1×10^{-4}	21
Calf, male	5	-4.9×10^{-4}	0.4×10^{-4}	8
Calf, female	6	-5.7×10^{-4}	1.4×10^{-4}	25

^aFor a given tissue type, we approximated $\mu_s'(\lambda)$ for each subject by fitting a linear function $a\lambda + b$ and the wavelength dependence of μ_s' then characterized by the ratio a/b . Column 3 shows this wavelength dependence estimator averaged over all subjects. Columns 4 and 5 show the corresponding standard deviation of this estimator both in absolute units and as a percentage of the estimator. Rows 1 and 2 show the results for the adult forearm and head (male and female mixed). Rows 3 to 5 show the results for the human calf; We obtained the results by pooling the male and female results and by segregating the data by sex.

two data sets, we recently repeated the measurements at a single wavelength (800 nm) on a new, larger group of subjects so as to provide a normalization point for the two earlier data sets. This determination of absolute μ_s' was validated on the solid phantom, as described in Section 4. Table 2 shows the mean and standard deviations for μ_s' measured at 800 nm on the forearm and calf of 14 adult volunteers (age range 23–42) and the heads of 10 volunteers (age range 23–35). The mean values of μ_s' have a typical standard deviation of 8%. Because the estimated accuracy of the measurement of interoptode spacing is ± 1 mm (i.e., $\pm 2.5\%$), and because from Eq. (1) it is evident that the derived value of μ_s' will vary approximately as $1/\rho^2$ for a given TPSF, interoptode spacing error will account for approximately 5% of this. For completeness, Table 2 also shows the resulting μ_a values. Figures 6(a)–6(c) show the averaged $\mu_s'(\lambda)$ spectra, normalized to the more recently determined average values at 800 nm. Table 3 shows the coefficients of the best-fit straight line to the data of Fig. 6 for the three tissue types. Also shown are the coefficients we obtained by fitting these spectra with a function of the form $y = b\lambda^{-a}$, i.e., the same function used by van Staveren *et al.* to model the unreduced scattering coefficient of Intralipid-10%. In all cases there is little difference

Table 2. Mean and Standard Deviations of the Absolute Value of μ_s' Measured on the Human Forearm, Intact Head, and Calf at 800 nm^a

Tissue Type	<i>n</i>	$\langle \mu_s' \rangle \pm \sigma(\mu_s')$ mm ⁻¹	$\langle \mu_a \rangle \pm \sigma(\mu_a)$ mm ⁻¹
Forearm	14	0.68 ± 0.08	0.023 ± 0.004
Intact head	10	0.94 ± 0.07	0.016 ± 0.001
Calf	14	0.94 ± 0.07	0.017 ± 0.005

^aAlso shown are the corresponding results for μ_a at 800 nm.

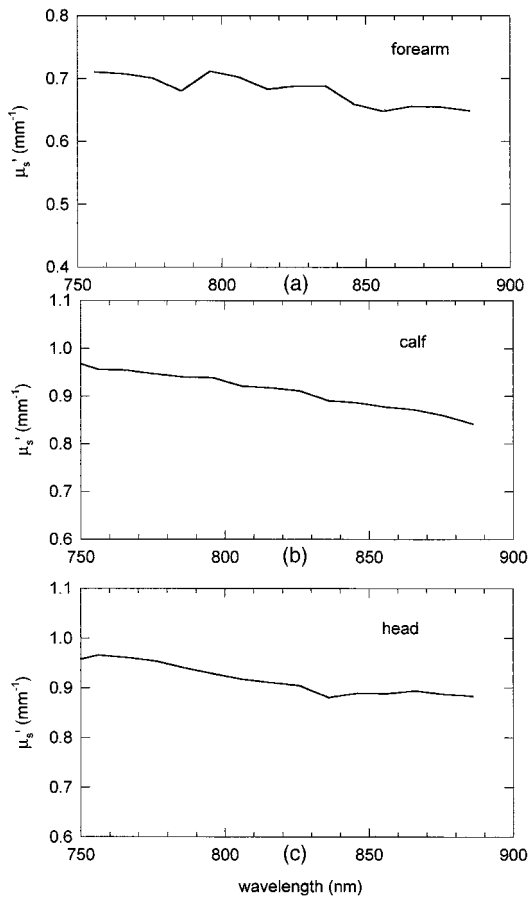


Fig. 6. $\mu_s'(\lambda)$ spectra averaged over all subjects and then normalized to the mean values at 800 nm reported in Table 2.

between this and the linear model, the linear model yielding marginally lower values for χ^2 .

6. Interpretation of the Results

To interpret the *in vivo* results, particularly for the head, one would clearly like to estimate the expected contribution of the various layers to the final derived value. This is clearly an extremely complicated task and one that we attempted to address here only in a simplified way. Specifically we used a time-dependent finite element model (FEM) of light transport in tissue²⁶ to generate TPSF's in the case of a model adult head. The model comprises two concentric circles of diameter 160 and 140 mm representing

Table 3. Wavelength Dependence of μ_s' for Three Tissue Types^a

Tissue Type	$\mu_s'(\lambda) = a\lambda + b$		$\mu_s'(\lambda) = b\lambda^{-a}$	
	a (mm ⁻¹ nm ⁻¹)	b (mm ⁻¹)	a	b
Forearm	-5.1×10^{-4}	1.1	0.576	32.48
Intact head	-6.5×10^{-4}	1.45	0.53	32.08
Calf	-8.9×10^{-4}	1.63	0.728	120.0

^aWe obtained the measurements by averaging the scattering coefficient spectra across all subjects, normalizing the values at 800 nm to those given in Table 2 and then fitting the $\mu_s'(\lambda)$ with both a linear function of wavelength $a\lambda + b$ and the function $b\lambda^{-a}$.

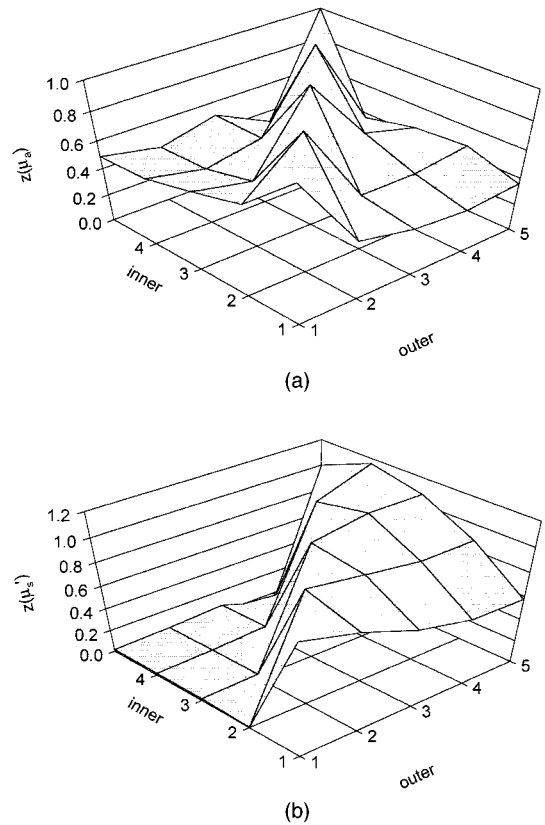


Fig. 7. Surface plots showing FEM simulations when we derived μ_a and μ_s' by TPSF fitting in the case of an inhomogeneous (two-layer) circle model. The numbers 1–5 on the x and y axes denote the optical properties used in the inner and outer regions of the model. The z axis denotes where the derived value lies between the inner and outer region values, i.e., 0 implies the value equals the lower of the two, 1.0 that it equals the higher, and 0.5 that it equals the mean of the two. (a) Results for μ_a ; (b) results for μ_s' .

skull and gray matter, respectively, i.e., the thickness of the skull layer is 1 cm. We then generated 25 TPSF's by varying the optical properties of the inner and surface regions independently using five different μ_a, μ_s' combinations: (1) $\mu_a = 0.01, \mu_s' = 0.5$ mm⁻¹; (2) $\mu_a = 0.0175, \mu_s' = 1.0$ mm⁻¹; (3) $\mu_a = 0.025, \mu_s' = 1.5$ mm⁻¹; (4) $\mu_a = 0.0325, \mu_s' = 2.0$ mm⁻¹; and (5) $\mu_a = 0.04, \mu_s' = 2.5$ mm⁻¹. These model TPSF's were then fitted with the use of the homogeneous Patterson equation. Figure 7 shows the results in the form of surface plots. The x and y axes are labeled with numbers (between 1 and 5) that represent the μ_a, μ_s' combinations assigned to the outer and inner regions in a particular TPSF calculation. The z axis plots the derived value of the optical property in relation to the limits defined by the inner and outer region properties. Specifically, if we generate a TPSF using optical properties $(\mu_a, \mu_s')_1$ and $(\mu_a, \mu_s')_2$ for the two regions that yields derived optical properties $(\mu_a, \mu_s')_d$, whereas using these properties uniformly throughout the model yields derived properties $(\mu_a, \mu_s')_{1d}$ or $(\mu_a, \mu_s')_{2d}$, then the z

value (for μ_a) would be

$$z = \frac{(\mu_{ad} - \mu_{a1d})}{(\mu_{a2d} - \mu_{a1d})},$$

where $(\mu_a, \mu_s')_{1d} < (\mu_a, \mu_s')_{2d}$. Hence a value of 0.0 indicates that the derived value equals the lower of the inner-outer values whereas 1.0 indicates that it equals the higher value. Values below 0.0 or above 1.0 indicate that the derived value lies outside the range defined by the inner and outer values. Values along the line $x = y$ (where the TPSF's are calculated with a homogeneous FEM model) are assigned arbitrarily the value 1.0.

Referring to Fig. 7(a), one can see that for all the combinations used, the derived value of μ_a lies between the values for the inner and outer region (apart from the $x = y$ line, as mentioned). Thus on the basis of this simple model, we are inclined to interpret our derived μ_a values as a mean of the *in vivo* values for skull and gray matter. Figure 7(b) shows rather different behavior. First, although the majority of combinations yield derived μ_s' values that lie within the upper and lower limits, there are a few combinations that yield μ_s' 16% higher than the upper limit. Second, the form of the surface shows that the derived μ_s' value rarely can be regarded as an average of the values for the two layers. Instead the derived value appears to track the value of the outer region more closely than in the case of μ_a . Although more detailed modeling clearly is needed, this result suggests that the *in vivo* μ_s' values derived with time-resolved spectroscopy applied to the adult head with 40-mm probe spacing may be indicative primarily of μ_s' of the surface tissues. Our results should be viewed in this light.

7. Discussion

To within the level of fluctuation introduced by inter-subject variability, all three tissue types exhibit a broadly similar wavelength dependence of μ_s' . This wavelength dependence is comparatively weak; the decrease in μ_s' from 760 to 900 nm is less than 10% in all three tissues. To increase confidence that we are measuring the wavelength dependence of the transport coefficients accurately, we can also consider the wavelength dependence of the derived absorption coefficient. It is currently assumed by several groups that the absorption coefficient of tissue consists almost entirely of absorption that is due to oxy-hemoglobin, deoxyhemoglobin, and water. With this assumption, we can estimate the hemoglobin saturation in the tissue by performing a multicomponent analysis³⁴ on the μ_a spectra using the spectra of lysed hemoglobin (oxy and deoxy) and pure water. When we performed this analysis on the μ_a spectra for the forearm, head, and calf (averaged over subjects) over the wavelength range 760–880 nm, it yielded the results shown in Table 4. Because the fitted range does not include the main water peak at 975 nm, we would not expect to derive an accurate concentration for water. One can see from the table that our in-

Table 4. Derived Concentrations of Hb and HbO₂ (μM)^a

	Hb/HbO ₂ Fit		Hb/HbO ₂ /H ₂ O Fit		
	Hb (μM)	HbO ₂ (μM)	Hb (μM)	HbO ₂ (μM)	H ₂ O (%)
Forearm	42	75	42	84	-14
Intact head	28	50	28.2	57	-12
Calf	26	58	27	60	-4

^aWe obtained measurements by fitting the derived tissue $\mu_a(\lambda)$ with the spectra of lysed Hb and HbO₂ and also with these spectra plus the spectrum of pure H₂O.

cluding water in the fit has a small effect on the derived HbO₂ concentration but yields slightly (<14%) negative apparent H₂O concentrations. In either case the derived hemoglobin saturations [HbO₂/(HbO₂ + Hb)] of 64–67%, 64–67%, and 69%, respectively, are reasonable physiologically and encourage us to believe that the wavelength dependence of the transport coefficients are measured accurately.

Our results for the calf and forearm, where the majority of the probed tissue should be skeletal muscle, appear somewhat different from the *in vitro* results for muscle currently available. Cheong *et al.* reviewed the published data obtained on bovine muscle using various measurement techniques,¹¹ quoting typical values for μ_a (0.04–0.35 mm⁻¹ at 630 nm, 0.12 mm⁻¹ at 1064 nm, 0.23 mm⁻¹ at 1320 nm) and μ_s' (0.44–0.7 mm⁻¹ at 633 nm, 0.28 mm⁻¹ at 1064 nm, 0.24 mm⁻¹ at 1320 nm). Eddowes reported values obtained using coherent backscatter measurements at 1064 nm ($\mu_a = 0.058 \pm 0.007$ mm⁻¹, $\mu_s' = 0.58 \pm 0.06$ mm⁻¹).¹⁶ Our results for μ_s' appear significantly higher than values quoted for bovine muscle by Cheong *et al.*, but are closer to those reported by Eddowes, given the estimated wavelength dependence of μ_s' . Our results for μ_a are much lower than the quoted *in vitro* values for bovine muscle. This discrepancy may be plausible at 630 nm because μ_a at this wavelength will have a large contribution from cytochromes but is less plausible at 1064 nm. This wavelength lies at a trough in the water absorption spectrum, and the *in vivo* value of μ_a at this wavelength should be only 20–30% higher than at 800 nm if Hb, HbO₂, and H₂O are the dominant absorbers in tissue. Our *in vivo* estimates of μ_s' for the head appear significantly lower than expected based on *in vitro* measurements. Sterenborg *et al.* used an integrating sphere technique together with Kubelka-Munk theory of light transport to measure $\mu_a(\lambda)$ and $\mu_s'(\lambda)$ on *in vitro* samples of cerebral gray and white matter together with tumor samples.³⁵ For gray matter they estimate μ_s' at 800 nm to be approximately 4 mm⁻¹. van der Zee also measured $\mu_a(\lambda)$ and $\mu_s'(\lambda)$ on *in vitro* adult human cerebral gray matter with Monte-Carlo modeling of measured diffuse reflectance and transmittance, obtaining values of approximately 0.032 mm⁻¹ and 2.4 mm⁻¹, respectively, at 800 nm¹² for bloodless samples. Firbank *et*

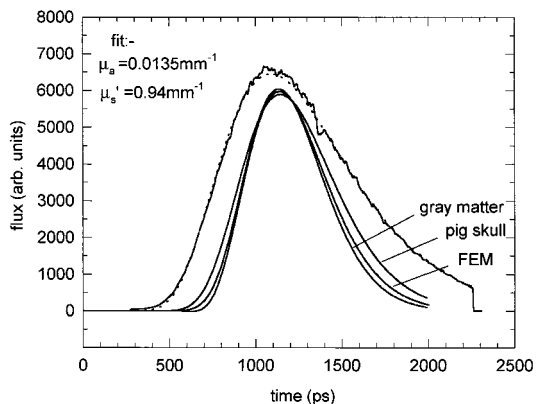


Fig. 8. Comparison of a TPSF measured across 43 mm of adult head with three theoretical TPSF's. The first two TPSF's were generated with Eq. (1) with the *in vitro* estimates of the optical properties of (a) pig skull cortical bone and (b) adult human cerebral gray matter plus a contribution for blood. The third TPSF was generated with a FEM model of light propagation in a heterogeneous three-layer head model. This model uses the above *in vitro* μ_s' estimates for bone and gray matter plus an *in vitro* estimate of μ_s' for adult human cerebral white matter.¹²

al. performed measurements, using an identical apparatus as van der Zee, on bloodless samples of adult pig skull cortical bone, obtaining values of 0.025 mm^{-1} and 1.8 mm^{-1} , respectively, at 800 nm .²⁷ To illustrate the discrepancy between these values and the *in vivo* data, Fig. 8 shows a comparison between an actual TPSF measured across 43 mm of adult head and three theoretical TPSF's. Two of these TPSF's were generated with Eq. (1) for μ_a , μ_s' values of 0.047, 2.4 and 0.032, and 1.8 mm^{-1} (blood-perfused adult human cerebral gray matter and adult pig skull cortical bone, respectively). The third was generated with the FEM model of light transport³⁶ across 43 mm of a 160-mm-diameter three-layer head model (the three layers were skull, gray matter, and white matter), which incorporated the same optical properties as before plus van der Zee's *in vitro* estimate of white matter μ_a , μ_s' (0.0034 mm^{-1} , 8.4 mm^{-1}) (plus an appropriate contribution for $80 \mu\text{M}$ of hemoglobin). The TPSF's are visibly quite different from the experimental data in that the measured TPSF has a significantly larger FWHM than the model TPSF's (note that the amplitudes of the model TPSF's are arbitrary). Interestingly, however, the mean times of all TPSF's are similar, ranging from 1203 ps for the gray matter model, through 1228 ps for the FEM-generated TPSF, to 1277 ps for the measured TPSF. To a first order, the mean time of a TPSF is determined by the ratio of μ_s' to μ_a , hence a measured mean time is compatible with a wide range of μ_a , μ_s' values. Thus, although our existing data for mean time measured across the adult head is compatible with our *in vitro* estimates of brain and skull transport coefficients, the present analysis suggests that both μ_a and μ_s' may be overestimated in the *in vitro* work. It is possible that the presence of a clear layer of cerebrospinal fluid between the skull and the ce-

rebral cortex distorts the propagation of light sufficiently to account for this outcome. The precise effect of such a clear layer is currently the subject of investigation.³⁷ We note, however, that our results, particularly for absorption coefficient, are also different significantly from published values for forearm and calf skeletal muscle where no clear layer is present. These discrepancies may indicate that the scattering and absorption properties of tissue vary considerably between the *in vivo* and the *in vitro* cases or alternatively that the currently available *in vitro* estimates are unreliable. Torres *et al.* suggested that current estimates for the μ_a of aortic wall tissue obtained with spectrophotometric methods are too high (by as much as a factor 5) to be compatible with the observed rate of surface tissue heating that is due to laser irradiation.³⁸ Graaff *et al.* reported substantial inconsistencies between *in vitro* transport coefficient values available in the literature for human skin and measurements of the radial variation of diffuse back reflectance measured *in vivo* on the human finger,³⁹ finding that the *in vivo* measurements suggest substantially lower values for both μ_a and μ_s' . For cerebral tissues, our *in vivo* results seem consistent with values of transport scattering coefficient and absorption coefficient that are significantly lower than the *in vitro* values currently available in the literature. For skeletal muscle, our scattering coefficient values are somewhat higher than published *in vitro* values, whereas our absorption coefficient values are much lower. These results are comparable with those reported by Zaccanti *et al.* at 825 nm with an essentially identical technique²² [averaged over five subjects, Zaccanti *et al.* report: forearm (μ_a , μ_s') = (0.0236 ± 0.002 , 0.55 ± 0.1); head (0.0147 ± 0.001 , 0.84 ± 0.09); calf (0.023 ± 0.002 , 0.68 ± 0.1) mm^{-1}]. Our results thus add support to the case that the currently available *in vitro* tissue optical properties are largely unreliable, either because after excision the tissue properties are altered by storage and handling procedures or because the original measurement techniques are flawed. If true, these finding will have an important bearing on the accurate modeling of the performance of near-infrared imaging and spectroscopy techniques as well as photodynamic therapies.

We thank Hamamatsu Photonics KK, the Wellcome Trust, and the Engineering and Physical Sciences Research Council for generous financial support. We thank Mike Firbank, David Hall, and Jeremy Hebden for useful discussions. We also acknowledge the help of numerous members of the research team in collecting the original set of wavelength-dependent TPSF's used in this research.

References and Notes

1. F. F. Jöbsis, "Non-invasive, infrared monitoring of cerebral and myocardial oxygen sufficiency and circulatory parameters," *Science* **198**, 1264–1267 (1977).
2. J. S. Wyatt, M. Cope, D. T. Delpy, S. Wray, and E. O. R. Reynolds, "Quantitation of cerebral oxygenation and haemo-

- dynamics in sick newborn infants by near infrared spectroscopy," *Lancet* **8515**, 1063–1066 (1986).
3. M. Ferrari, C. De Marchis, I. Giannini, A. Nicola, R. Agostino, S. Nodari, and G. Bucci, "Cerebral blood volume and haemoglobin oxygen saturation monitoring in neonatal brain by near infrared spectroscopy," *Adv. Exp. Med. Biol.* **200**, 203–212 (1986).
 4. B. C. Wilson and M. S. Patterson, "The physics of photodynamic therapy," *Phys. Med. Biol.* **31**, 327–360 (1986).
 5. S. R. Arridge, P. van der Zee, M. Cope, and D. T. Delpy, "Reconstruction methods for infra-red absorption imaging," in *Time-Resolved Spectroscopy and Imaging of Tissues*, B. Chance and A. Katzir, eds., *Proc. SPIE* **1431**, 204–215 (1991).
 6. D. A. Benaron and D. K. Stevenson, "Optical time-of-flight and absorbance imaging in biologic media," *Science* **259**, 1463–1466 (1993).
 7. M. S. Patterson, B. C. Wilson, and D. R. Wyman, "The propagation of optical radiation in tissue. I. Models of radiation transport and their application," *Lasers Med. Sci.* **6**, 155–167 (1990).
 8. M. S. Patterson, E. Schwartz, and B. C. Wilson, "Quantitative reflectance spectrophotometry for the non-invasive measurement of photosensitizer concentration in tissue during photodynamic therapy," in *Photodynamic Therapy: Mechanisms*, T. J. Dougherty, ed., *Proc. SPIE* **1065**, 115–122 (1989).
 9. S. J. Matcher, P. Kirkpatrick, K. Nahid, M. Cope, and D. T. Delpy, "Absolute quantification methods in tissue near infrared spectroscopy," in *Optical Tomography: Photon Migration, and Spectroscopy of Tissue and Model Media: Theory, Human Studies, and Instrumentation*, B. Chance and R. R. Alfano, eds., *Proc. SPIE* **2389**, 486–495 (1995).
 10. H. Liu, D. A. Boas, Y. Zhang, A. G. Yodh, and B. Chance, "Simplified approach to characterize optical properties and blood oxygenation in tissue using continuous near-infrared light," in *Optical Tomography: Photon Migration, and Spectroscopy of Tissue and Model Media: Theory, Human Studies, and Instrumentation*, B. Chance and R. R. Alfano, eds., *Proc. SPIE* **2389**, 496–502 (1995).
 11. W. F. Cheong, S. A. Prahl, and A. J. Welch, "A review of the optical properties of biological tissues," *IEEE J. Quantum Electron.* **26**, 2166–2185 (1990).
 12. P. van der Zee, "Measurement and modelling of the optical properties of human tissue in the near-infrared," Ph.D dissertation (University of London, London, 1992).
 13. S. T. Flock, B. C. Wilson, and M. S. Patterson, "Total attenuation coefficients and scattering phase functions of tissues and phantom materials at 633 nm," *Med. Phys.* **14**, 835–841 (1987).
 14. B. C. Wilson, T. J. Farrell, and M. S. Patterson, "An optical-fiber based diffuse reflectance spectrometer for non-invasive investigation of photodynamic sensitizers *in vivo*," in *Future Directions and Applications in Photodynamic Therapy*, C. J. Gomer, ed., *SPIE Institute Series* **IS06**, 219–231 (1990).
 15. G. Yoon, D. N. Ghosh Roy, and R. C. Straight, "Coherent backscattering in biological media: measurement and estimation of optical properties," *Appl. Opt.* **32**, 580–585 (1993).
 16. M. Eddowes, "Coherent backscatter and its use in measuring the optical properties of biological tissues," Ph.D dissertation (University of London, London, 1995).
 17. J. M. Schmitt, A. Knüttel, and R. F. Bonner, "Measurement of optical properties of biological tissues by low-coherence reflectometry," *Appl. Opt.* **32**, 6032–6042 (1993).
 18. M. S. Patterson, B. Chance, and B. C. Wilson, "Time resolved reflectance and transmittance for the non-invasive measurement of tissue optical properties," *Appl. Opt.* **28**, 2331–2336 (1989).
 19. M. Barilli, G. Zaccanti, P. Brusciaglioni, A. Ismaelli, Q. N. Wei, and M. Ferrari, "Optical properties of *in vivo* human skeletal muscle from near infrared picosecond laser pulse," in *Photodynamic Therapy and Biomedical Lasers*, P. Spinelli, M. Dal Fante, and R. Marchesini, ed. (Elsevier, New York, 1992), pp. 930–934.
 20. G. Mitic, J. Kölzer, J. Otto, E. Plies, G. Sölkner, and W. Zinth, "Time-gated transillumination of biological tissues and tissue-like phantoms," *Appl. Opt.* **33**, 6699–6710 (1994).
 21. K. Suzuki, Y. Yamashita, K. Ohta, and B. Chance, "Quantitative measurement of optical parameters in the breast using time-resolved spectroscopy," *Invest. Radiol.* **29**, 410–414 (1994).
 22. G. Zaccanti, A. Taddeucci, M. Barilli, P. Brusciaglioni, and F. Martelli, "Optical properties of biological tissues," in *Optical Tomography: Photon Migration, and Spectroscopy of Tissue and Model Media: Theory, Human Studies, and Instrumentation*, B. Chance and R. R. Alfano, eds., *Proc. SPIE* **2389**, 513–521 (1995).
 23. M. Essenpreis, C. E. Elwell, M. Cope, P. van der Zee, S. R. Arridge, and D. T. Delpy, "Spectral dependence of temporal point spread functions in human tissues," *Appl. Opt.* **32**, 418–425 (1993).
 24. S. J. Madsen, B. C. Wilson, M. S. Patterson, Y. D. Park, S. L. Jacques, and Y. Hefetz, "Experimental tests of a simple diffusion model for the estimation of scattering and absorption coefficients of turbid media from time-resolved diffuse reflectance measurements," *Appl. Opt.* **31**, 3509–3517 (1992).
 25. R. C. Haskell, L. O. Svaasand, T. Tsay, T. Feng, M. S. McAdams, and B. J. Tromberg, "Boundary conditions for the diffusion equation in radiative transfer," *J. Opt. Soc. Am. A* **11**, 2727–2741 (1994).
 26. M. Schweiger, "Application of the finite element method in infrared image reconstruction of scattering media," Ph.D dissertation (University of London, London, 1994).
 27. M. Firbank, M. Hiraoka, and D. T. Delpy, "Measurement of the optical properties of the skull in the wavelength range 650–950 nm," *Phys. Med. Biol.* **38**, 503–510 (1993).
 28. H. J. van Stavaren, C. J. M. Moes, J. van Marle, S. A. Prahl, and M. J. C. van Gemert, "Light scattering in Intralipid-10% in the wavelength range 400–1100 nm," *Appl. Opt.* **30**, 4507–4514 (1991).
 29. M. Firbank and D. T. Delpy, "A design for a stable and reproducible phantom for use in near infra-red imaging and spectroscopy," *Phys. Med. Biol.* **38**, 847–853 (1993).
 30. Y. Pan, R. Engelhardt, J. Rosperich, G. Hüttmann, and R. Birngruber, "Measurement of optical transport coefficients of Intralipid in visible and NIR range," in *Laser-Tissue Interaction V*, S. L. Jacques, ed., *Proc. SPIE* **2134A**, 353–364 (1994).
 31. J. T. Allardice, A. Mutaz Abulafi, D. G. Webb, and N. S. Williams, "Standardization of Intralipid for light scattering in clinical photodynamic therapy," *Lasers Med. Sci.* **7**, 461–465 (1992).
 32. M. Cope, D. T. Delpy, S. Wray, J. S. Wyatt, and E. O. R. Reynolds, "A CCD spectrometer to quantitate the concentration of chromophores in living tissue utilising the absorption peak of water at 975 nm," *Adv. Exp. Med. Biol.* **247**, 33–40 (1989).
 33. Numerical Algorithms Group Mk 16, Numerical Algorithms Group Ltd, Wilkinson House, Jordan Hill Road, Oxford OX2 8DR UK.
 34. M. Cope, "The development of a near infrared spectroscopy system and its application for non-invasive monitoring of cerebral blood and tissue oxygenation in the newborn infant," Ph.D dissertation (University of London, London, 1991).
 35. H. J. C. M. Sterenborg, M. J. C. van Gemert, W. Kamphorst, J. G. Wolbers, and W. Hogervorst, "The spectral dependence of the optical properties of human brain," *Lasers Med. Sci.* **4**, 221–227 (1989).
 36. S. R. Arridge, M. Schweiger, M. Hiraoka, and D. T. Delpy, "A

- finite element approach for modelling photon transport in tissue," *Med. Phys.* **20**(2), 299–309 (1993).
37. M. Firbank, M. Schweiger, and D. T. Delpy, "Investigation of light piping through clear regions of scattering objects," in *Optical Tomography: Photon Migration, and Spectroscopy of Tissue and Model Media: Theory, Human Studies, and Instrumentation*, B. Chance and R. R. Alfano, eds., *Proc. SPIE* **2389**, 167–173 (1995).
38. J. H. Torres, A. J. Welch, I. Çilesiz, and M. Motamedi, "Tissue optical property measurements: overestimation of absorption coefficient with spectrophotometric techniques," *Lasers Surg. Med.* **14**, 249–257 (1994).
39. R. Graaff, A. C. M. Dassel, M. H. Koelink, F. F. M. de Mul, J. G. Aarnoudse, and W. G. Zijlstra, "Optical properties of human dermis *in vitro* and *in vivo*," *Appl. Opt.* **32**, 435–447 (1993).